WRC RESEARCH REPORT NO. 44

METHODOLOGY FOR SYNTHESIS AND OPTIMIZATION OF DIFFUSION PATTERNS IN FLOW SYSTEMS

by

W. Hall C. Maxwell
Associate Professor of Civil Engineering
and
Kuo-Cheng Chang
Research Assistant in Civil Engineering

University of Illinois at Urbana-Champaign

FINAL REPORT

Project No. A-046-ILL

July 1, 1970 — June 30, 1971

The work upon which this publication is based was supported by funds provided by the U.S. Department of the Interior as authorized under the Water Resources Research Act of 1964, P.L. 88-379
Agreement No. 14-31-0001-3213

UNIVERSITY OF ILLINOIS
WATER RESOURCES CENTER
2535 C. E. Hydrosystems Lab.
Urbana, Illinois 61801

July 1971

ABSTRACT

METHODOLOGY FOR SYNTHESIS AND OPTIMIZATION OF DIFFUSION PATTERNS IN FLOW SYSTEMS

This analytic study used a generalization of Reichardt's hypothesis by Alexander, Baron & Comings to develop a unified treatment for the synthesis of diffusion patterns for mass, heat and momentum. The technique was applied for co-planar and co-axial flows, to a study of the effects of initial flux distribution and outlet shape on diffusion patterns; and to shallow submerged outlets. Four simple approximations to the P-function, involving only exponential and error functions, were found to represent flux distributions downstream from a circular jet of finite size at all points between the nozzle and infinity.

The results may be applied in the study and design of discharge outlets, syphon spillways, hydraulic breakwaters and diffusion of tracers in streams and penstocks.

Maxwell, W. Hall C., and Chang, Kuo-Cheng
METHODOLOGY FOR SYNTHESIS AND OPTIMIZATION OF DIFFUSION PATTERNS IN FLOW SYSTEMS
Completion Report to Office of Water Resources Research, Department of the Interior, Washington, D.C., July 1970, 46 pp.
KEYWORDS—*boundaries (surfaces)/ *diffusion/ flow characteristics/ *flow profiles/ fluid flow/ *free surfaces/ free turbulence/ heat flux/ hydraulics/ *jets/ mass flux/ momentum flux/ similarities/ temperature/ tracers

CONTENTS

LIST OF FIGURES

LIST OF TABLES

NOTATION

The following symbols are used in this report:

a = $\sqrt{3}/6$ times side of equilateral triangular nozzle

A = constant of proportionality, Eq. 5

A_o = efflux area of jet

b_ψ = general jet width parameter

b = jet width parameter for momentum flux, or horizontal dimension of rectangular nozzle

B = constant of proportionality, Eq. 7

c_p = specific heat of fluid

C_ψ = general spreading coefficient

C = spreading coefficient for momentum flux

d = vertical dimension of rectangular nozzle

D_E = equivalent diameter for non-circular nozzle

D = diameter of nozzle or height of slot

$f(x,y)$ = function of x and y, Eq. 4

$f(\eta)$ = function of η, Eq. 62

$F(z)$ = function of z, Eq. 56

$G(\eta)$ = function of η, Eq. 60

$g(s)$ = strength of line source jet, Eq. 2

$H(\frac{\bar{u}_m}{U_1}, \frac{\bar{u}_o}{U_1})$ = function defined by Eq. 23

$I_o(r)$ = modified Bessel function, argument r

j = exponent or coefficient; j = 0 for plane-symmetry; j = 1 for axial symmetry

k = constant, Table 1

ℓ_m = characteristic length, Eq. 20

m = subscript denoting axial values, except for ℓ_m and x_m

n = exponent, Eq. 5

o = subscript denoting efflux value, except for x_o

p = dummy variable, Eq. 47

$P(\chi^2|2,\lambda)$ = non-central chi-square probability function, with two degrees of freedom and non-centrality parameter λ

$P(\chi^2|\nu)$ = chi-square probability function with ν degrees of freedom

$P(R,r)$ = P-function, Eq. 65 and Eq. 66

$P^*(R,r)$ = normalized P-function, Eq. 67

r = $2ys/(C_\psi x)^2$ in Eq. 38, or argument of P-function = $\sqrt{2}y/(C_\psi x)$

R = argument of P-function = $D/(\sqrt{2}\ C_\psi x)$

s = radial polar co-ordinate in plane of nozzle discharge or rectangular co-ordinate in y direction in plane of slot discharge

t = dummy variable, Eq. 46

u = instantaneous velocity in x-direction

u' = fluctuation from time mean value of u

U_1 = velocity of co-axial or co-planar flow

v = instantaneous velocity in y-direction

w_i = concentration of i^{th} component; mass per unit fluid mass

x = co-ordinate in direction of jet axis

x_m = measured value of x

x_s = value of x at which maximum flux reaches free surface

x_o = zero correction or origin shift for x

y = co-ordinate normal to slot edge for plane symmetry; radial co-ordinate for axial symmetry; lateral rectangular co-ordinate for shallow submerged jet

z = vertical rectangular co-ordinate

z_o = vertical submergence of nozzle centerline below free surface

z_m = vertical co-ordinate of maximum flux

δ = increment

η = dimensionless vertical distance, Eq. 57

θ = small angular deflection of jet

θ_1 = temperature difference from ambient at a point in the fluid

λ = non-centrality parameter for non-central chi-square probability function, $= 2y^2/(C_\Psi{}^2x^2)$

ν = degrees of freedom for chi-square probability function, Eq. 30

ρ = fluid density

χ^2 = argument of non-central chi-square distribution, Eq. 27

$\Psi = \rho w_i$ for mass flux; $= \rho C_p \theta_1$ for heat flux; $= \rho u$ for momentum flux.

I. INTRODUCTION

Previous research by the principal investigator (1,2,3)[1] has examined techniques for the analysis of jet flow patterns influenced by various boundary conditions. A generalization of Reichardt's (4) hypothesis by Alexander, Baron & Comings (5) permitted solutions to be obtained for complex flow patterns. Moreover, diffusion of momentun, mass and heat flux could be analyzed in a unified manner. Velocity distributions could be readily predicted from the momentum flux solutions by neglecting axial turbulent velocity fluctuations. Of particular relevance to the present investigation was a technique for the determination of the influence of finite nozzle size on the flux pattern just downstream from a jet nozzle. The initial uniform distribution at the nozzle mouth was represented as a distribution of infinitesimal point jet sources of flux of equal strength. This led to solutions which could be approximated using readily available statistical tables. A logical extension of this work is to examine the possibility of reproducing prescribed flux patterns, such as might exist in river channels or penstocks, by using distributions of point or line source jets of unequal strength. By introducing the concept of image sources of "negative flux" there is the possibility that flux patterns near solid boundaries could be simulated. The use of image source of positive flux had proved successful in predicting the influence of a free surface on flux patterns for shallow submerged jets (2). The diffusion of "negative flux" into the real flow field could accommodate the added constraint that momentum flux is not conserved near a solid boundary.

---

[1] Numerals in parentheses refer to corresponding items in List of References.

The initial objective of the present investigation was therefore to investigate methods for synthesizing logarithmic or power law profiles using distributions of line or point sources of flux of different strength as a basic building block. The results of that investigation are presented in the following section.

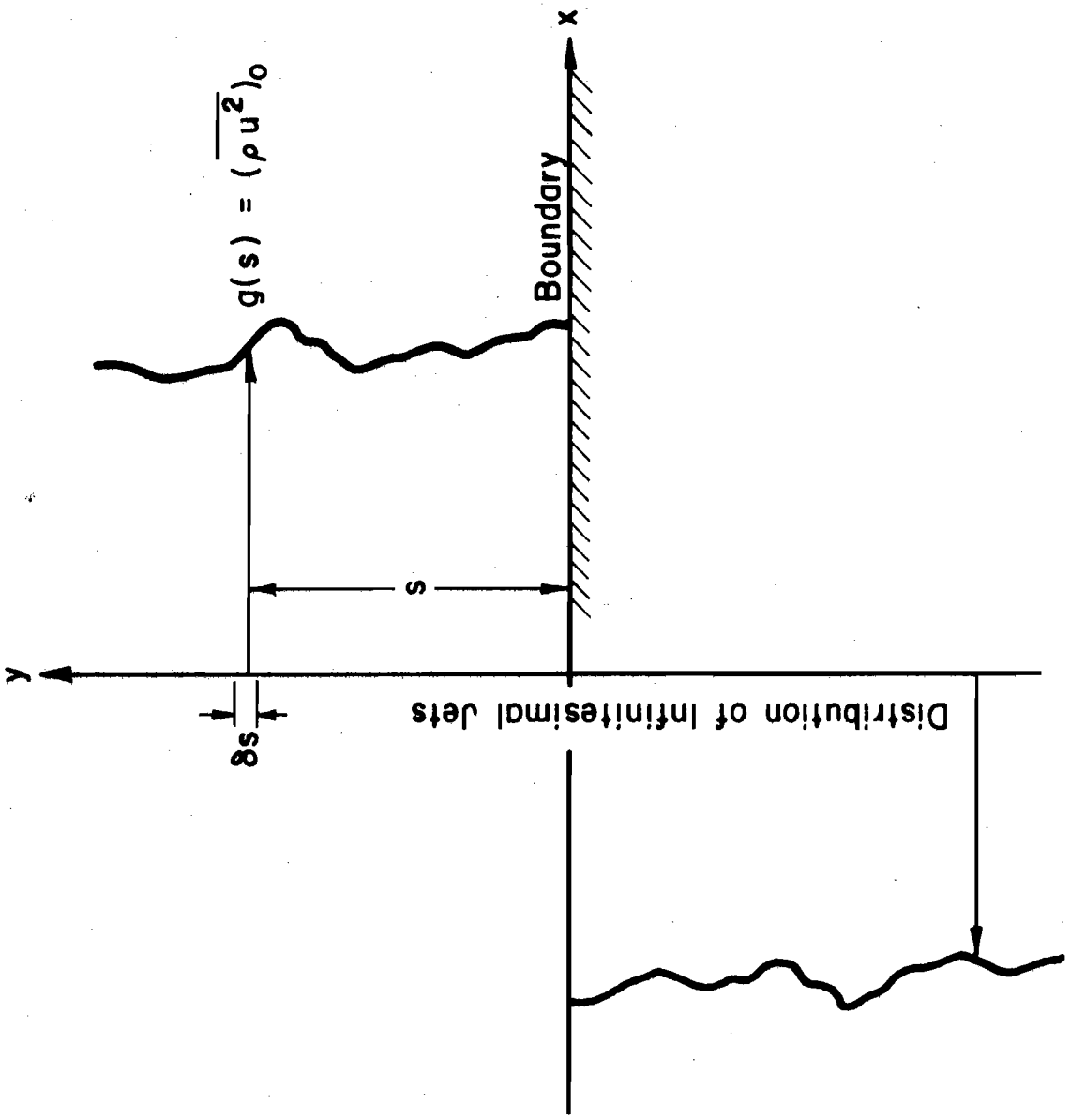

Fig. 1 - Schematic Representation of Infinitesimal Jet Distribution

II. TECHNIQUES FOR PROFILE SYNTHESIS

With reference to Fig. 1 the momentum flux at (x,y) due to an elementary line source jet of strength $(\overline{\rho u^2})_o$ and area = (δs x 1), located at (o,s) is given by (3)

$$\delta[\overline{\rho u^2}] = \frac{1}{\sqrt{\pi}\, Cx} \; (\overline{\rho u^2})_o \exp[-(y-s)^2/(Cx)^2]\delta s \tag{1}$$

Letting

$$(\overline{\rho u^2}) = g(s) \tag{2}$$

to indicate that the strength of a line source jet is a function of its position, the flux downstream from a distribution of line source jets is then obtained by integration of Eq. 1

$$\overline{\rho u^2} = \frac{1}{\sqrt{\pi}\, Cx} \int_{-\infty}^{\infty} g(s) \exp[-(y-s)^2/(Cx)^2]ds \tag{3}$$

Herein ρ = fluid density; u = instantaneous velocity in the x direction; x = co-ordinate parallel to the boundary; y = co-ordinate normal to the boundary; C = spreading coefficient for momentum flux; s = dummy variable along the y-axis; bars denote time averages; and o = subscript referring to values at x = 0.

From Eq. 3 $\overline{\rho u^2}$ is seen to be a function of x and y. Useful solutions will be those for which $\overline{\rho u^2}$ is independent of x. Eq. 3 may be written

$$f(x,y) = \frac{1}{\sqrt{\pi}\, Cx} \int_{-\infty}^{\infty} g(s)\, \exp[-(y-s)^2/(Cx)^2]ds \qquad (4)$$

The basic problem is to solve Eq. 4 for g(s) when f(x,y) is prescribed and independent of x. Various methods for accomplishing this were investigated, including Fourier Transforms (6) and Bilateral Laplace Transforms (7). In addition various forms of g(s) were assumed and the corresponding f(x,y) evaluated using Eq. 4.

For fully developed flows near a rigid boundary a power law distribution of velocity may be assumed.

$$\overline{u} = Ay^{\frac{1}{n}} \qquad (5)$$

in which A is a constant of proportionality and the n in the exponent may assume various values depending on the Reynolds number. (n generally lies between 6 and 10) (8). If it is assumed that the effect of the longitudinal fluctuations of velocity, u' may be neglected

$$\overline{\rho u^2} \simeq \rho \overline{u}^2 \qquad (6)$$

Then, for constant density

$$\overline{\rho u^2} \simeq By^{\frac{2}{n}} \qquad (7)$$

in which B is a new constant of proportionality. Eq. 4 then becomes

$$By^{\frac{2}{n}} = \frac{1}{\sqrt{\pi}\, Cx} \int_{-\infty}^{\infty} g(s)\, \exp[-(y-s)^2/(Cx)^2]ds \qquad (8)$$

The solution of Eq. 6 was investigated for all positive integer values of n. No finite solutions could be found for $n \geq 3$, which in effect eliminates those solutions which would be of practical interest. The solutions for n = 1 and n = 2 may be readily verified by substitution in Eq. 8 so that none of the mathematics used will be detailed here. Table I summarizes solutions which were found.

From Table I it is seen that only the simplest transformation g(s) = ks yields a momentum flux distribution which is independent of x. The method therefore holds little promise for simulating flux patterns which do not spread. In view of this the emphasis during the remainder of the investigation was placed on synthesizing flux patterns which do spread.

TABLE I — The Transformation $f(x,y) = \frac{1}{\sqrt{\pi}Cx} \int_{-\infty}^{\infty} g(s) \exp[-(\frac{y-s}{Cx})^2]ds$

k = constant

f(x,y)	g(s)
ky	ks
ky^2	$k(s^2 - \frac{C^2x^2}{2})$
$k \operatorname{erf}(\frac{y}{Cx})$	$k, s \geq o$ $-k, s \leq o$ }
$k \sum_{\delta=o}^{N} \frac{n!}{(n-2\delta)!\ \delta!} \frac{1}{2^{2\delta}} (\frac{y}{Cx})^{n-2\delta}$ $N = \frac{n}{2}$, for n even $= \frac{n-1}{2}$, for n odd	$k(\frac{s}{Cx})^n$
$k \exp(\frac{C^2x^2}{4}) \sinh y$	$k \sinh s$
$k \exp(\frac{C^2x^2}{4}) \cosh y$	$k \cosh s$
$k \exp(-\frac{C^2x^2}{4}) \sin y$	$k \sin s$
$k \exp(-\frac{C^2x^2}{4}) \cos y$	$k \cos s$

III. FLUX SOURCES IN CO-AXIAL AND CO-PLANAR FLOWS

One problem in which spreading does occur is that for which a source of momentum flux lies in a co-axial or co-planar flow. Such a situation exists where, for example, tracers are injected into penstocks to permit in situ calibration of turbines in hydroelectric plants during acceptance tests. Various investigators (9, 10, 11, 12) have collected data on the diffusion of momentum when jets of fluid are injected into co-planar or co-axial flows. Such data lends itself to analysis by the method of synthesis used here.

The basic equation for this method is (2, 3)

$$\frac{\partial \overline{\Psi u}}{\partial x} - \frac{1}{y^j} \frac{b_\Psi}{2} \frac{d\, b_\Psi}{dx} \frac{\partial}{\partial y} \left(y^j \frac{\partial \overline{\Psi u}}{\partial y}\right) = 0 \tag{9}$$

in which $j = 0$ for plane symmetry and $j = 1$ for axial symmetry. For mass flux, $\Psi = \rho w_i$, in which ρ = fluid density and w_i = concentration of the i^{th} component expressed as mass per unit mass of fluid; for heat flux, $\Psi = \rho c_p \theta_i$, in which c_p = specific heat of the fluid and θ_i = temperature difference from ambient at a point in the fluid; for momentum flux, $\Psi = \rho u$. b_Ψ = a general jet width parameter. For an infinitesimal jet

$$b_\Psi = C_\Psi x \tag{10}$$

in which C_Ψ is constant and is called the spread coefficient. For momentum flux $C_\Psi = C$.

The basic equation for momentum flux with constant density is (2, 3)

$$\frac{\partial \overline{u^2}}{\partial x} + \frac{1}{y^j}\frac{\partial}{\partial y}\left(y^j \overline{uv}\right) = 0 \tag{11}$$

in which v = the instantaneous velocity parallel to the y-axis in rectangular co-ordinates and in the radial direction for cylindrical co-ordinates.

The lateral distribution for a point or line source of flux at any given x can be shown to be (2, 3)

$$\frac{\overline{\Psi u}}{(\overline{\Psi u})_m} = \exp\left[-(y/b_\Psi)^2\right] \tag{12}$$

in which the subscript m refers to the value on the axis. The corresponding axial distribution of flux is

$$\frac{(\overline{\Psi u})_m}{(\overline{\Psi u})_o} = \frac{A_o}{(\sqrt{\pi} b_\Psi)^{j+1}} \tag{13}$$

in which A_o = area of a slot of unit width for j = 0, or = area of a circular orifice for j = 1.

The axial distribution of flux for a jet of finite size can then be shown by synthesis to be (2, 3)

$$\frac{(\overline{\Psi u})_m}{(\overline{\Psi u})_o} = \operatorname{erf}\left(\frac{D}{2C_\Psi x}\right) \text{ for plane symmetry}$$

$$= 1 - \exp\left[-\left(\frac{D}{2C_\Psi x}\right)^2\right] \text{ for axial symmetry} \tag{14}$$

For a jet in a co-axial or co-planar stream with uniform velocity U_1, performing an integration normal to the axis over an area which extends to $y_o > b$, it can be shown, using an argument similar to that presented by Naudascher (13) that Eq. 9 implies that:

$$\frac{d}{dx}\left\{\int_o^{y_o} \overline{\Psi u}\, 2(\pi y)^j\, dy\right\} = 0 \tag{15}$$

Following the same procedure with Eq. 11 for the momentum flux yields:

$$\frac{d}{dx}\left\{\int_o^{y_o} \rho\overline{(u-U_1)u}\, 2(\pi y)^j\, dy\right\} = 0 \tag{16}$$

Hence, for co-axial or co-planar jet flows

$$\Psi = \rho(u-U_1) \tag{17}$$

From Eq. 12

$$\frac{\overline{\rho\, u\, (u-U_1)}}{[\overline{\rho\, u\, (u-U_1)}]_m} = \exp\,[-(y/b)^2] \tag{18}$$

Assuming that ρ is constant and that $\overline{\rho u'^2}$ may be neglected this reduces to

$$\frac{\overline{u}\,(\overline{u}-U_1)}{\overline{u}_m\,(\overline{u}_m-U_1)} = \exp\,[-(y/b)^2] \tag{19}$$

Naudascher (13) defined a characteristic length

$$\ell_m^{j+1} = \int_o^\infty \frac{\bar{u}\ (\bar{u}-U_1)}{\bar{u}_m\ (\bar{u}_m-U_1)}\ (2y)^j\ dy \tag{20}$$

Substituting Eq. (19) in Eq. (20) it follows that

$$\ell_m = \left(\frac{2}{\sqrt{\pi}}\right)^j \frac{\sqrt{\pi}}{2} \cdot b \tag{21}$$

In Fig. 3 of Ref. 13, Naudascher has in effect presented a plot for Eq. 13 compared with data by Ortega (11) for an axisymmetric jet in a co-axial field for $12 \leq x/D \leq 96$ and obtained good agreement. No data are shown closer to the nozzle than 12 diameters so that the point source model of Eq. 19 can be expected to provide good correlation.

Bradbury (12) has presented measurements in a slot jet in a co-planar field. From Eq. 14, again assuming negligible $\overline{\rho u'^2}$ and constant ρ

$$\frac{\bar{u}_m\ (\bar{u}_m-U_1)}{\bar{u}_o\ (\bar{u}_o-U_1)} = \operatorname{erf} \frac{D}{2Cx} \tag{22}$$

This may be converted to the form:

$$\frac{x}{D} = \frac{1}{2C}\left[\operatorname{arc\ erf}\left\{\frac{\frac{\bar{u}_m}{U_1}\left(\frac{\bar{u}_m}{U_1}-1\right)}{\frac{\bar{u}_o}{U_1}\left(\frac{\bar{u}_o}{U_1}-1\right)}\right\}\right]^{-1} = \frac{1}{2C} H\left(\frac{\bar{u}_m}{U_1}, \frac{\bar{u}_o}{U_1}\right) \tag{23}$$

Moreover, from Eq. 13

$$\frac{\bar{u}_m\ (\bar{u}_m-U_1)}{\bar{u}_o\ (\bar{u}_o-U_1)} = \frac{D}{\sqrt{\pi}b} \tag{24}$$

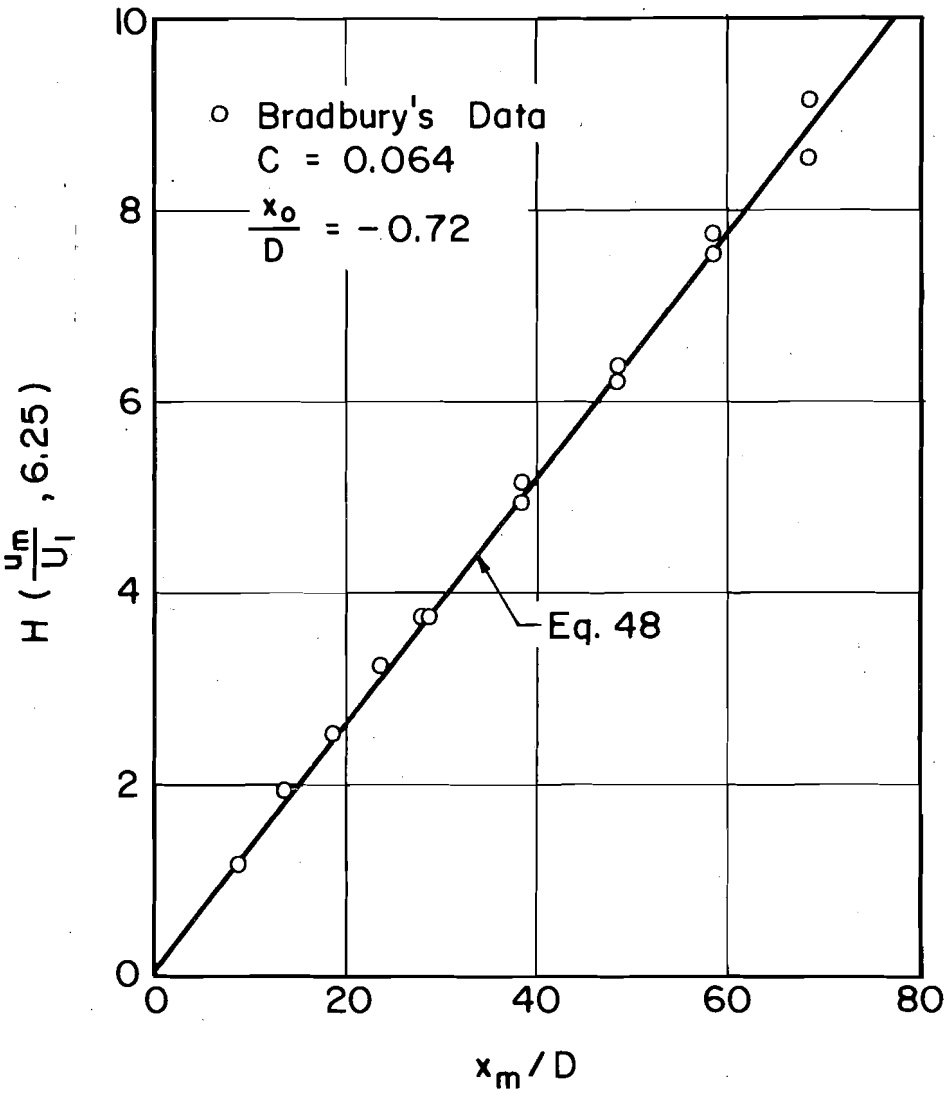

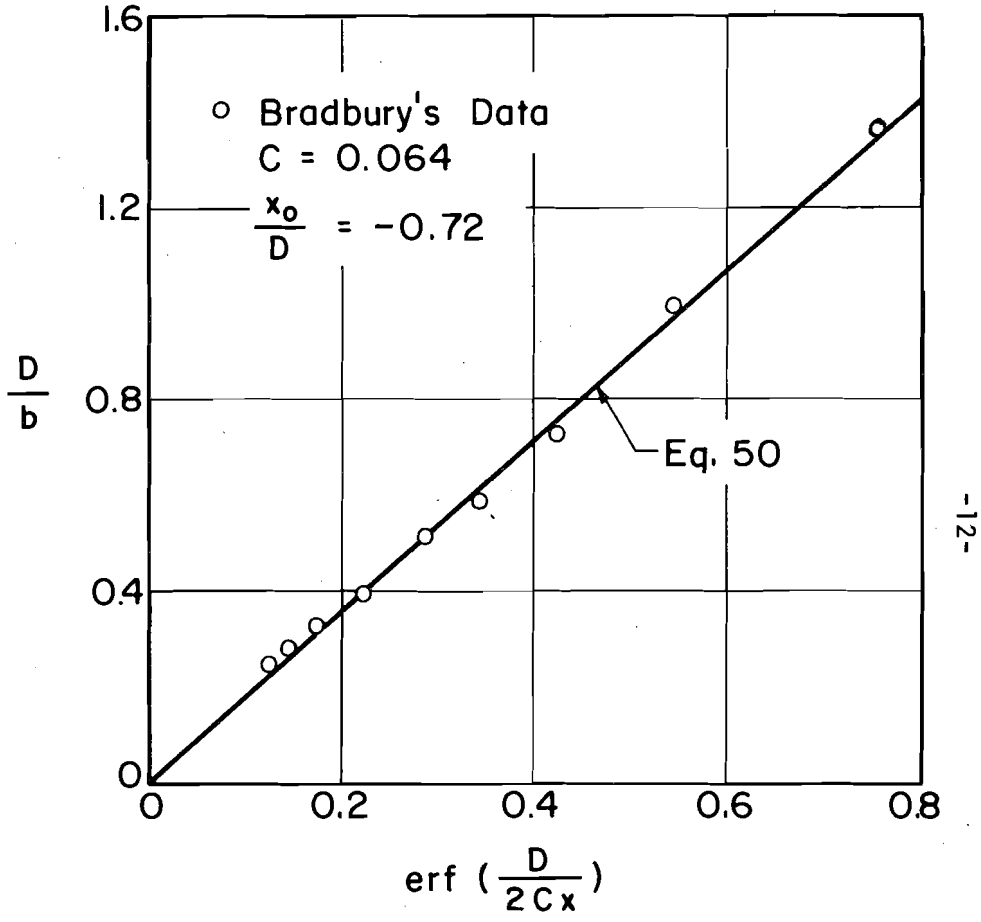

Fig. 2 - Variation of Jet Width and Center Line Velocity for Plane-Symmetric Jet in Co-planar Flow; Bradbury (12) Data

Combining Eq. 22 and Eq. 24

$$\frac{D}{b} = \sqrt{\pi}\ \mathrm{erf}\ \frac{D}{2Cx} \tag{25}$$

Fig. 2 shows a comparison of Eq. 23 and 25 with Bradbury's data with C = 0.064 and $x_o/D = -0.72$. Note that x_m refers to the measured value of x and x_o to the zero correction such that

$$x = x_m - x_o \tag{26}$$

In Fig. 6 of Ref. 14, Naudascher has, again, in effect presented a plot of Eq. 19 compared with data by Curtet and Ricou (10) for an axisymmetric jet in a co-axial field for $5 \leq x/D \leq 45$. In this case good agreement was obtained for $10 \leq x/D \leq 45$, as would be expected for the point source model of Eq. 19. Correlation for x/D = 5 was poor. An improved model which takes into account the finite size of the jet nozzle is given (2, 3) by the cumulative distribution function ofthe non-central chi-square distribution with two degrees of freedom and non-centrality parameter $2y^2/(C_\Psi{}^2x^2)$. Letting

$$\chi^2 = \frac{1}{2(C_\Psi x/D)^2} \quad \text{and} \quad \frac{y}{D} = \sqrt{\frac{\lambda}{2}}\,\frac{C_\Psi x}{} \tag{27}$$

This may be written

$$\frac{\overline{\Psi u}}{(\overline{\Psi u})_o} = P(\chi^2 | 2, \lambda) \tag{28}$$

One of the available approximations to the non-central chi-square distribution is the chi-square approximation with ν degrees of freedom. Eqs. 28 may be written

$$\frac{\overline{\Psi u}}{(\overline{\Psi u})_o} = P(\chi^2|2,\lambda) \approx P(\frac{\nu}{2+\lambda}\chi^2|\nu) \tag{29}$$

in which the quantity on the right hand side is a chi-square distribution function with

$$\nu = \frac{(2+\lambda)^2}{2(1+\lambda)} \tag{30}$$

Hence, for the axisymmetric flow case considered here, using Eq. 17 and again assuming ρ = constant and that $\overline{\rho u'^2}$ may be neglected

$$\frac{\overline{u}\ (\overline{u}-U_1)}{\overline{u}_o\ (\overline{u}_o-U_1)} \approx P(\frac{\nu}{2+\lambda}\chi^2|\nu) \tag{31}$$

Moreover, the axial flux distribution is given by Eq. 14 as

$$\frac{\overline{u}_m\ (\overline{u}_m-U_1)}{\overline{u}_o\ (\overline{u}_o-U_1)} = 1 - \exp\left[-(\frac{D}{2Cx})^2\right] \tag{32}$$

This may be written as

$$\frac{x}{D} = \frac{1}{2C}\left\{-\ell n\left[1 - \frac{\overline{u}_m\ (\overline{u}_m-U_1)}{\overline{u}_o\ (\overline{u}_o-U_1)}\right\}^{-1/2}\right. \tag{33}$$

Thus, a plot of x/D versus the bracketed root on the right-hand side of Eq. 33 should be linear. Its slope will determine C and the intercept

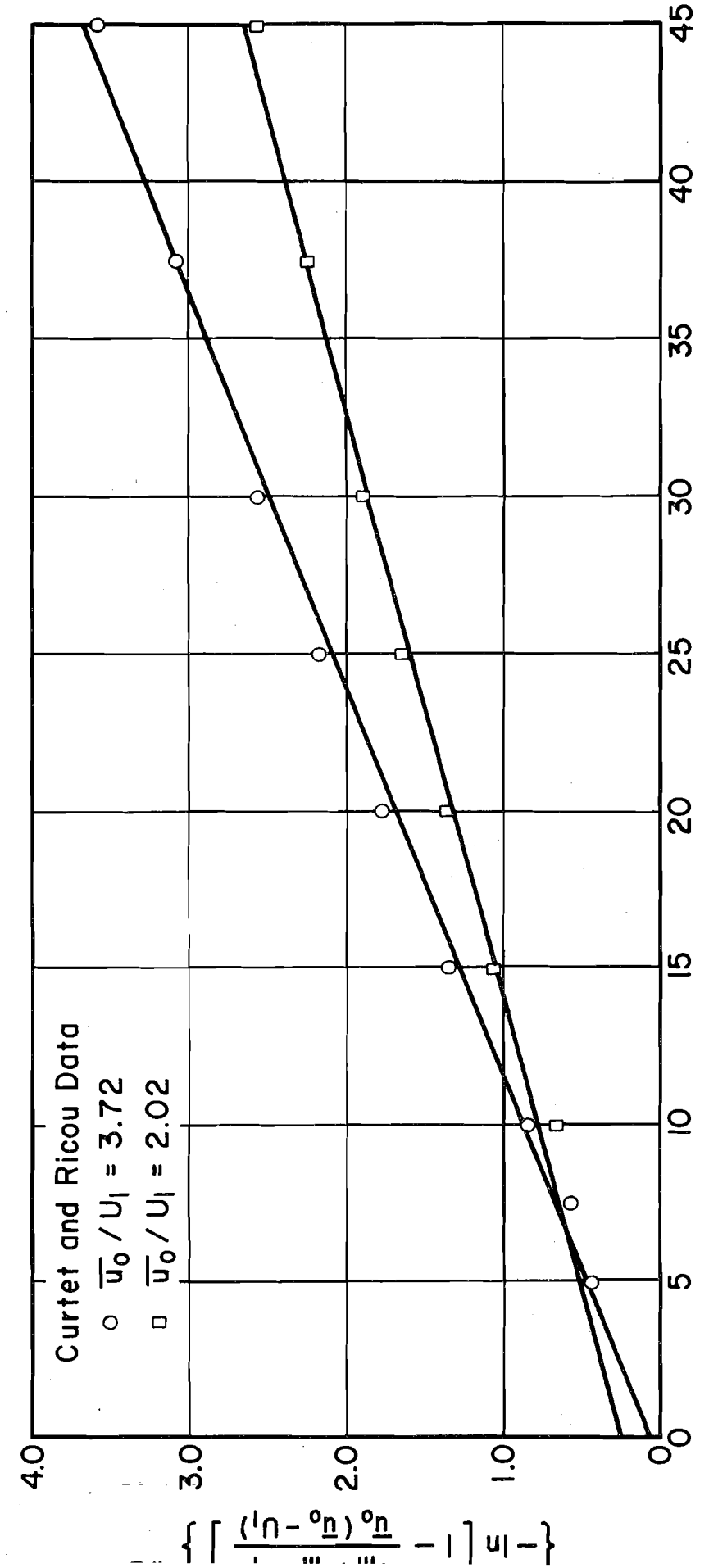

Fig. 3 - Axial Variation of Momentum Flux for Axisymmetric Jet in Co-axial Stream; Curtet and Ricou Data (14)

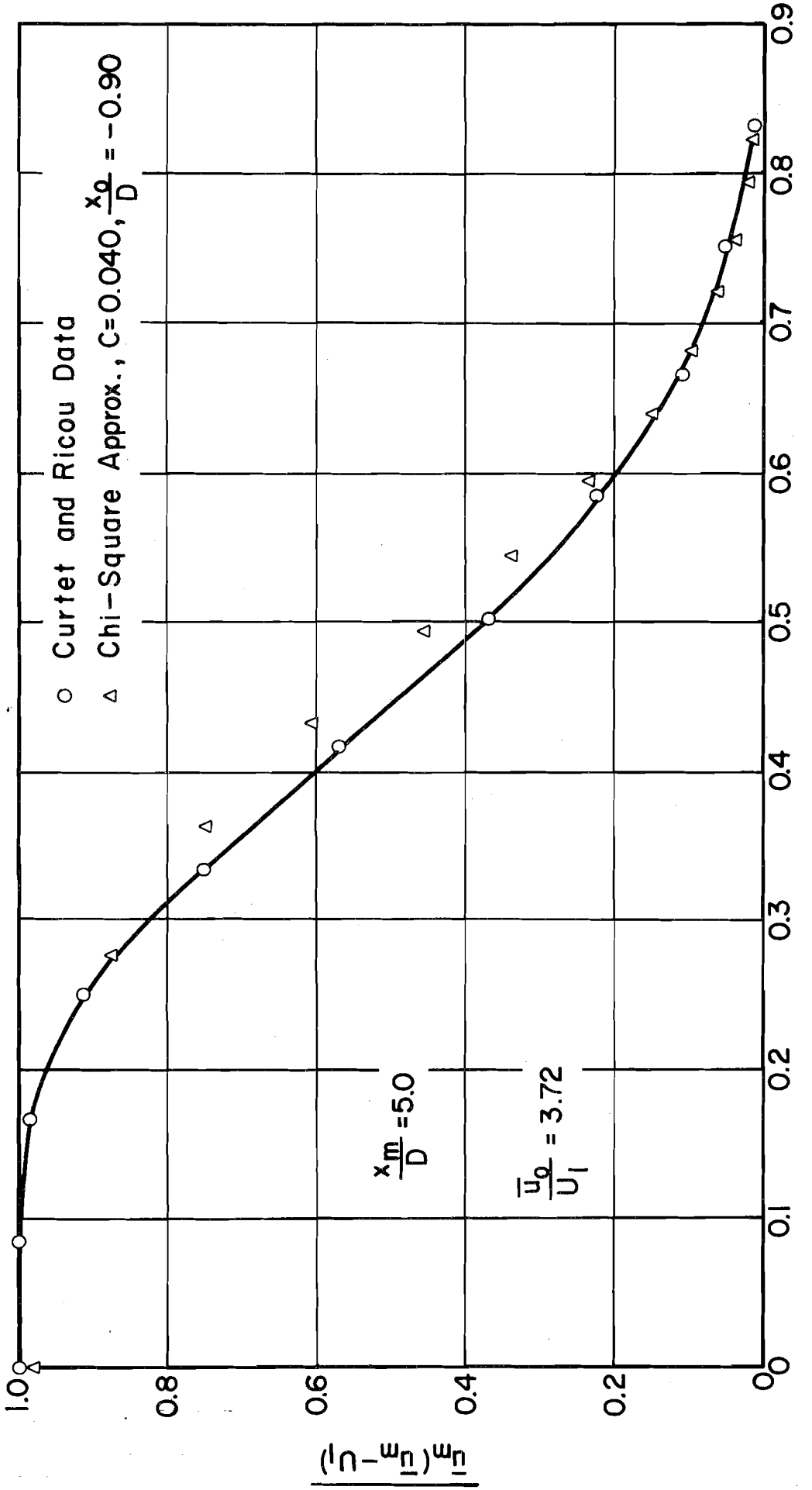

Fig. 4 - Transverse Variation of Momentum Flux for Axisymmetric Jet In Co-axial Stream; Curtet and Ricou Data (14); $x_m/D = 5.0$

on the x/D axis will determine the zero correction, x_o/D. Fig. 3 shows such a plot of two sets of axial data by Curtet and Ricou (10) taken from Table 2 of Ref. 14. Both C and x_o are seen to depend on $\overline{u}_o/U_1$.

Transverse data for $x_m/D = 5$, $\overline{u}_o/U_1 = 3.72$ were taken from Fig. 5 of Ref. 14. From a least squares fit of the corresponding axial data shown in Fig. 3 herein, $C = 0.040$ and $x_o/D = -0.90$. Using these values the chi-square approximation to the lateral distribution was computed and is compared with the data in Fig. 4. While agreement is not perfect the correlation shows substantial improvement over that obtained in Fig. 6 of Ref. 14. It should be noted that the development of Eq. 31 assumes a uniform distribution of flux across the jet nozzle. The effects of non-uniformity of this distribution are considered in the next section.

IV. EFFECT OF INITIAL FLUX DISTRIBUTION

Theoretical studies on jet flow generally assume that discharge or flux at the outlet is uniformly distributed. In most experimental studies care is taken to make conditions at the outlet as uniform as possible. This may not be entirely realistic for application in water resources problems e.g. discharge from the submerged end of a long conduit, in which the boundary layer has become fully developed, will certainly not be uniform. It is generally assumed that, within a reasonable distance downstream from the outlet the diffusion pattern will not be much influenced by the initial distribution. The problem does not appear, however, to have been systematically investigated. The method of synthesis used herein offers a convenient means of investigating this effect.

Parallel to the 1/7-power law for velocity distribution assume a flux distribution given by

$$(\overline{\Psi u})_o = (\overline{\Psi u})_{o_m} (1-2s/D)^{2/7} \qquad \text{for } 0 \leq s \leq \frac{D}{2} \tag{34}$$

for both a plane-symmetric outlet of height D and an axisymmetric outlet of diameter D. The subscript m refers to the axial value. Defining the spatial mean value of $(\overline{\Psi u})_o$ as

$$\overline{(\overline{\Psi u})_o} = \frac{1}{A_o} \int_{A_o} (\overline{\Psi u})_o \, dA_o \tag{35}$$

with A_o = area of slot per unit length or area of orifice. Then

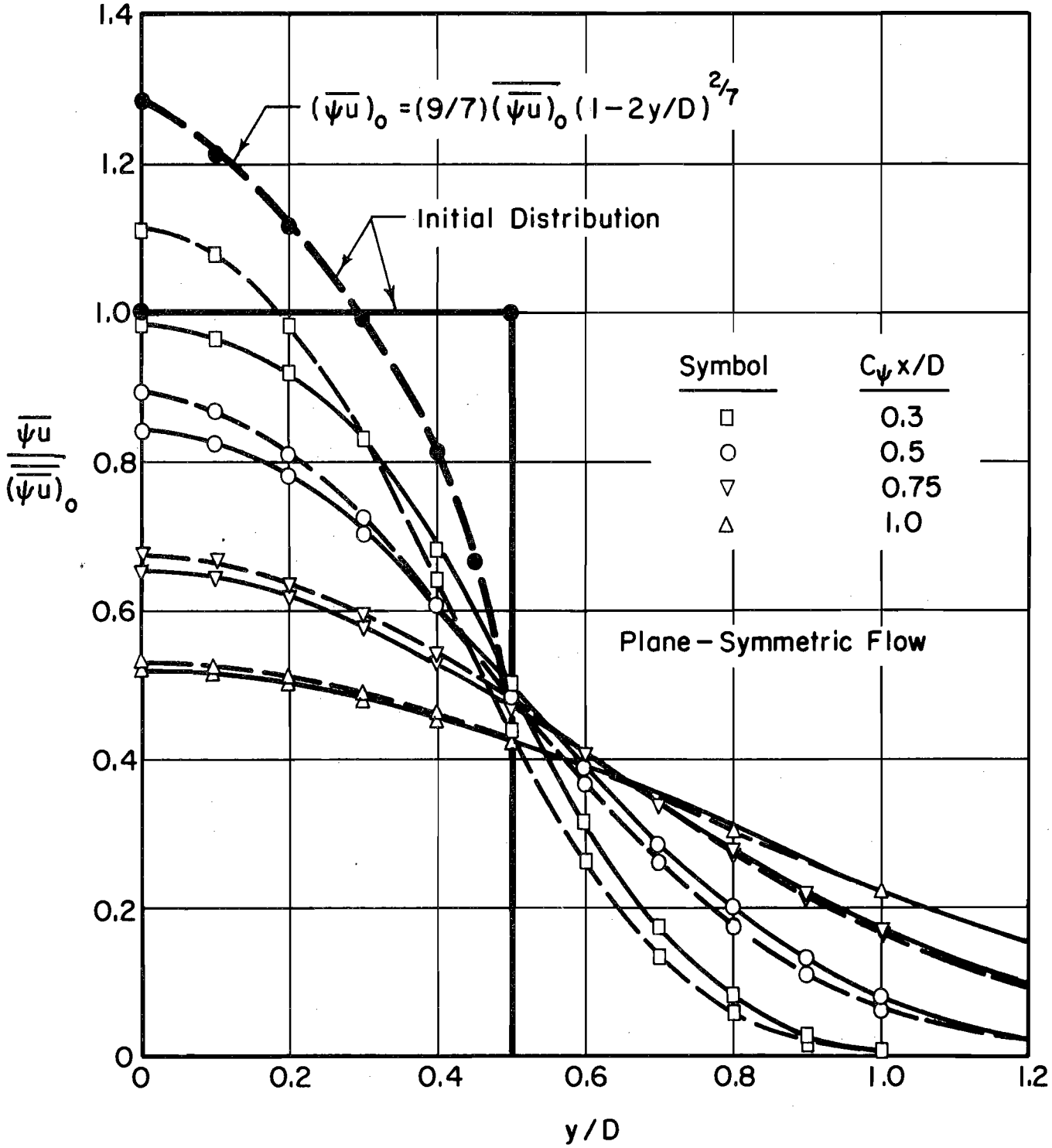

Fig. 5 - Effect of Initial Flux Distribution on Downstream Lateral Flux Distribution of a Plane-Symmetric Flow

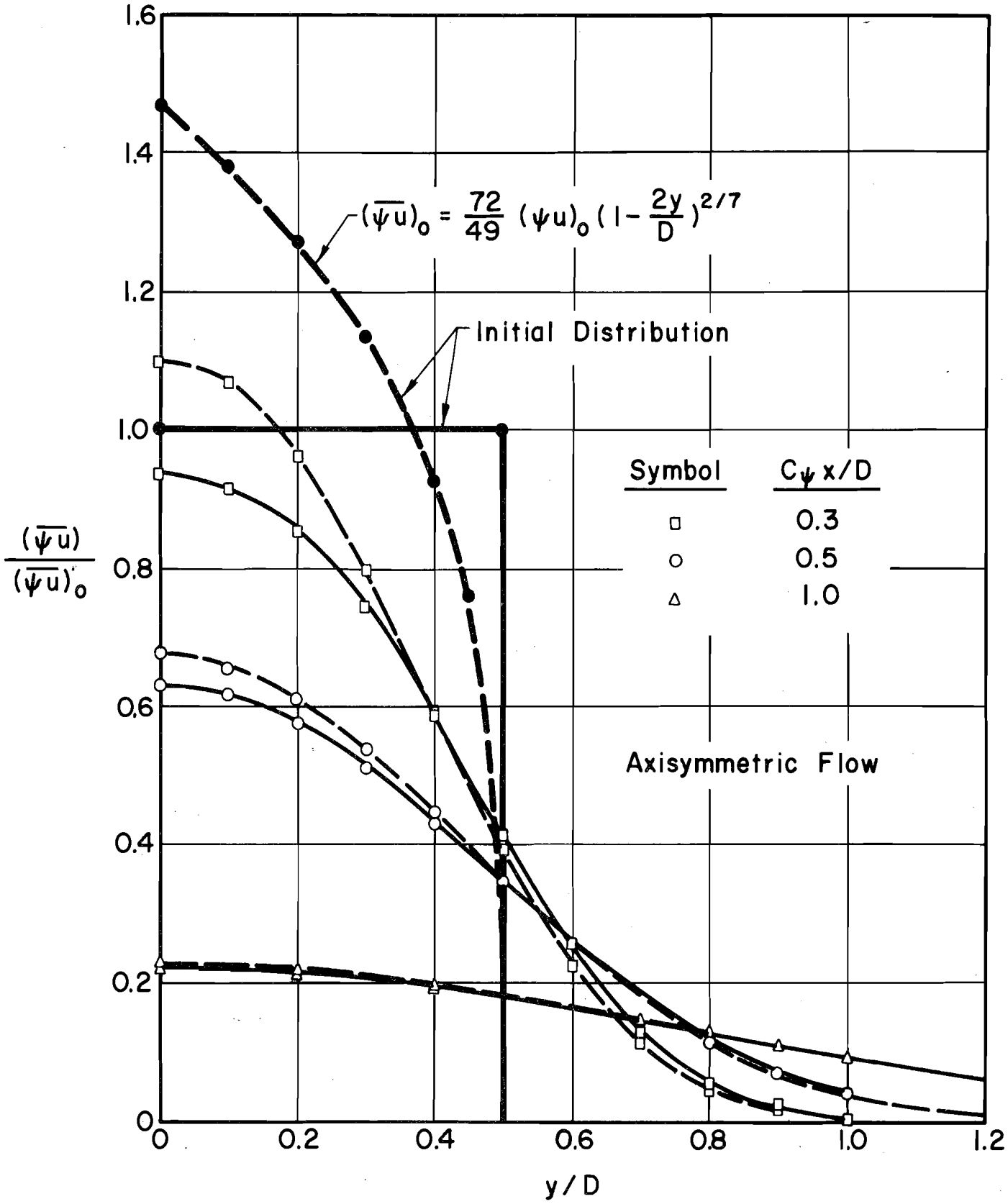

Fig. 6 - Effect of Initial Flux Distribution on Downstream Lateral Flux Distribution of an Axisymmetric Flow

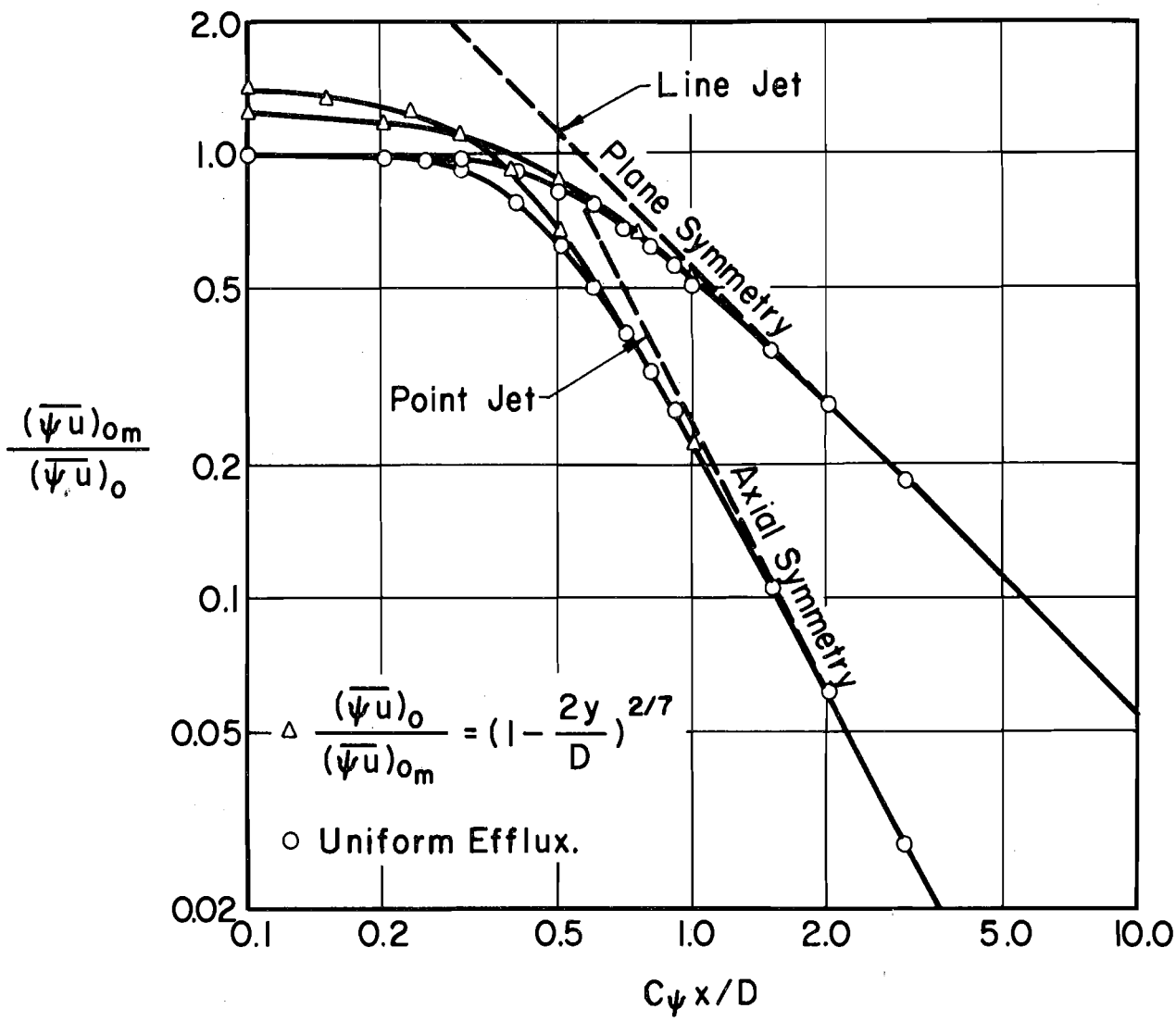

Fig. 7 - Effect of Initial Flux Distribution on Axial Flux Distribution for Plane- and Axisymmetric Flows

$$(\overline{\Psi u})_o = \left(\frac{8}{7}\right)^j \frac{9}{7} \overline{(\Psi \bar{u})_o} \, (1-2s/D)^{2/7} \tag{36}$$

The distribution of flux downstream from a jet of finite size is then given by (2, 3)

$$\overline{\Psi u} = \int_{A_o} (\overline{\Psi u})_o \frac{\exp\left[-\left(\frac{Y_{\delta A}}{C_\Psi x}\right)^2\right]}{(\sqrt{\pi} C_\Psi x)^{j+1}} \, dA \tag{37}$$

Substitution of Eq. 36 into Eq. 37 yields, after some manipulation

$$\frac{\overline{\Psi u}}{(\overline{\Psi u})_o} = \left(\frac{8\pi}{7}\right)^j \frac{18}{7} \frac{1}{(\sqrt{\pi} C_\Psi x)^{j+1}} \int_o^{\frac{D}{2}} (1-\tfrac{2s}{D})^{2/7} \exp\left[-\left(\frac{y-s}{C_\Psi x}\right)^2\right] \{s \exp(-r) I_o(r)\}^j \, ds \tag{38}$$

in which $r = 2ys/(C_\Psi x)^2$ and $I_o(r)$ is a modified Bessel function.

The integrals in Eq. 38 cannot be expressed in closed form. They were evaluated numerically and the results are plotted in Fig. 5, Fig. 6 and Fig. 7. Fig. 5 and Fig. 6 show the lateral flux distributions in comparison with those for a uniform efflux. Fig. 7 compares the longitudinal axial flux distributions with those of finite nozzles with uniform effluxes and with those for point and line source jets. It is seen that, for $C_\Psi x/D \geq 1.0$ the lateral flux distributions are virtually independent of the distribution at the outlet. For $C_\Psi x/D > 1.5$ both flux patterns are indistinguishable from those for point or line source jets.

V. EFFECT OF OUTLET SHAPE

Eq. 37 may also be used to determine whether or not the shape of the outlet has any significant influence on the downstream distribution flux. In view of the results in the last section the problem may be simplified by assuming that the flux distribution across the outlet is uniform. For the purposes of this analysis the y-co ordinate will be horizontal and normal to the longitudinal axis of symmetry, x; the z-co ordinate will be vertical and normal to the x-axis. The variables s and t will be dummy variables in the y and z directions respectively.

Consider a rectangular outlet of horizontal dimension b and vertical dimension d. Let the origin of co-ordinates be at the center of the rectangle. Then

$$dA = ds\ dt \tag{39}$$

and

$$y_{\delta A} = \{(y-s)^2 + (z-t)^2\}^{1/2} \tag{40}$$

with $-\frac{b}{2} \leq s \leq \frac{b}{2}$ and $-\frac{d}{2} \leq t \leq \frac{d}{2}$. Substituting Eq. 39 and Eq. 40 into Eq. 37 gives, after some manipulation

$$\frac{\overline{\Psi u}}{(\overline{\Psi u})_o} = \frac{1}{4}\left[\operatorname{erf}\left(\frac{b+2y}{2C_\Psi x}\right) + \operatorname{erf}\left(\frac{b-2y}{2C_\Psi x}\right)\right]\left[\operatorname{erf}\left(\frac{d+2z}{2C_\Psi x}\right) + \operatorname{erf}\left(\frac{d-2z}{2C_\Psi x}\right)\right] \tag{41}$$

Then, along the axis of symmetry (x, 0, 0)

$$\frac{(\overline{\Psi u})_m}{(\overline{\Psi u})_o} = \text{erf } (\frac{b}{2C_\Psi x}) \text{ erf } (\frac{d}{2C_\Psi x}) \tag{42}$$

Using a series expansion of Eq. 42 it is readily shown, that for large values of x

$$\frac{(\overline{\Psi u})_m}{(\overline{\Psi u})_o} \approx \frac{bd}{\pi C_\Psi^2 x^2} \tag{43}$$

Introducing the equivalent diameter

$$D_E = (\frac{4bd}{\pi})^{1/2} \tag{44}$$

Eq. 43 becomes identical to the distribution for a point source jet (2, 3)

$$\frac{(\overline{\Psi u})_m}{(\overline{\Psi u})_o} \approx \frac{D_E^2}{4C_\Psi^2 x^2} \tag{45}$$

The same result would, of course, apply to a square outlet, which is a special case of the rectangular solution (b=d).

Next, consider an equilateral triangle, of side $2\sqrt{3}$ a, with the origin of co-ordinates at its center of area and its vertex at (0, 0, 2a) Eq. 37 gives

$$\frac{\overline{\Psi u}}{(\overline{\Psi u})_o} = \frac{2}{\pi C_\Psi^2 x^2} \int_{-a}^{2a} \int_{o}^{(\frac{2a-t}{\sqrt{3}})} \exp\left[-\frac{(y-s)^2 + (z-t)^2}{C_\Psi^2 x^2}\right] ds\, dt \tag{46}$$

Along the x-axis

$$\frac{(\overline{\Psi u})_m}{(\overline{\Psi u})_o} = \frac{1}{\sqrt{\pi}} \int_{-\frac{a}{C_\Psi x}}^{\frac{2a}{C_\Psi x}} \text{erf}\left[\frac{1}{\sqrt{3}}\left(\frac{2a}{C_\Psi x} - p\right)\right] \exp(-p^2)\, dp \tag{47}$$

For large values of x expansion of Eq. 47 gives

$$\frac{(\overline{\Psi u})_m}{(\overline{\Psi u})_o} \approx \frac{3\sqrt{3}\, a^2}{\pi C_\Psi^2 x^2} \tag{48}$$

Again introducing the equivalent diameter

$$D_E = \left(\frac{\sqrt{3}}{\pi}\right)^{1/2} 2\sqrt{3}\, a \tag{49}$$

Eq. 49 reduces to Eq. 45, identical to the point source jet.

Eq. 41 and Eq. 47 have been evaluated for rectangles of different aspect ratios (b/d) and for the equilateral triangle and the results are listed in Table 2. It is seen that for values of $C_\Psi x/D_E > 5$ all the axial distributions are identical to that for a point source jet. For momentum flux a typical value of C is about 0.08. Thus axial momentum flux distributions beyond 63 diameters downstream from the outlet would not be affected by the shape of the outlet. From Fig. 7 it is seen that the effect of a non-uniform distribution of initial flux would be dissipated much closer to the outlet.

TABLE 2 — EFFECT OF OUTLET SHAPE ON AXIAL FLUX

$\frac{C_\psi x}{D_E}$	Value of $(\overline{\psi u})_m/(\overline{\psi u})_o$					
	Point Source Jet	Circular Jet	Equilateral Triangular Jet	Square Jet b/d = 1	Rectangular Jet b/d=0.2 or 5	Rectangular Jet b/d=0.1 or 10
0.10	—	1.000	1.000	1.000	0.995	0.952
0.20	—	0.998	0.991	0.997	0.839	0.678
0.30	—	0.938	0.900	0.928	0.650	0.491
0.40	—	0.790	0.747	0.779	0.516	0.380
0.50	1.000	0.632	0.599	0.624	0.423	0.308
0.75	0.444	0.359	0.347	0.356	0.273	0.207
1.00	0.250	0.221	0.216	0.220	0.185	0.150
1.50	0.111	0.105	0.104	0.105	0.096	0.086
2.00	0.063	0.061	0.061	0.061	0.058	0.054
3.00	0.028	0.027	0.027	0.027	0.027	0.026
3.50	0.020	0.020	0.020	0.020	0.020	0.019
4.00	0.016	0.016	0.016	0.016	0.015	0.015
5.00	0.010	0.010	0.010	0.010	0.010	0.010

VI. SHALLOW SUBMERGED SLOT OUTLETS

John, Mahajan & Kanbour (15) recently published data on flow and temperature patterns downstream from a slot set at various shallow submergences at the end of a narrow channel. In Ref. 2 an analytic model was developed for momentum flux patterns downstream from a shallow submerged circular jet set at various small angular deviations from the horizontal. The same techniques can be used to develop a more general model for momentum, mass and heat flux downstream from both axi-symmetric and plane-symmetric point or line source jet outlets.

From Eq. 12, with $b_\psi = C_\psi x$, the flux distributions are given by (2, 3)

$$\frac{\overline{\psi u}}{(\overline{\psi u})_m} = \exp\left[-\left(\frac{y}{C_\psi x}\right)^2\right] \tag{50}$$

in which y is a general co-ordinate for axi-symmetric and plane symmetric flows.

For a jet with a small initial upward deflection, θ, the mathematics may be considerably simplified by making the approximation

$$\frac{\overline{\psi u}}{(\overline{\psi u})_m} = \exp\left[-\left(\frac{r}{C_\psi x}\right)^2\right] \tag{51}$$

in which

$$r^2 = jy^2 + (z_o - z - \theta x)^2 \tag{52}$$

with z_o = distance of jet below z = 0, with z positive downwards; y is the lateral co-ordinate. This approximate model cannot be expected to apply for $x > z_o/\theta$.

Moreover, from Eq. 13

$$\frac{(\overline{\Psi u})_m}{(\overline{\Psi u})_o} = \left(\frac{2}{\sqrt{\pi}}\right)^{1-j} \left(\frac{D}{2C_\Psi x}\right)^{j+1} \tag{53}$$

For no flux across the free surface (which would restrict the application in the case of heat flux to situations where this would be a valid approximation) an image jet is placed equidistant above the surface to cancel the vertical flux when z = 0. The combination then gives

$$\frac{\overline{\Psi u}}{(\overline{\Psi u})_o} = \left(\frac{2}{\sqrt{\pi}}\right)^{1-j} \left(\frac{D}{2C_\Psi x}\right)^{j+1} \left\{\exp\left[-\frac{j\,y^2+(z_o-z-\theta x)^2}{C_\Psi^{\,2}x^2}\right]\right.$$

$$\left. + \exp\left[-\frac{j\,y^2+(z_o+z-\theta x)^2}{C_\Psi^{\,2}x^2}\right]\right\} \tag{54}$$

After some manipulation this may be written

$$\frac{\overline{\Psi u}}{(\overline{\Psi u})_o} = \left(\frac{2}{\sqrt{\pi}}\right)^{1-j} \left(\frac{D}{2C_\Psi x}\right)^{j+1} \exp\left[-j\left(\frac{y}{C_\Psi x}\right)^2\right] \exp\left[-\left(\frac{z_o-\theta x}{C_\Psi x}\right)^2\right] F(z) \tag{55}$$

in which

$$F(z) = \exp\left[-\left(\frac{z}{C_\Psi x}\right)^2\right] \cosh\left[\frac{2z(z_o-\theta x)}{C_\Psi^{\,2}x^2}\right] \tag{56}$$

The location of the maximum flux is obtained by setting z = 0 in Eq. 55 and maximizing $\overline{\Psi u}/(\overline{\Psi u})_o$ with respect to z. This yields identical results

results for axi-symmetric and plane symmetric flows, namely with

$$\eta = \frac{z_m}{z_o - \theta x} \tag{57}$$

with z_m = the vertical co-ordinate of the maximum flux.

$$\eta = \tanh\left[2\eta\left(\frac{z_o - \theta x}{C_\psi x}\right)^2\right] \tag{58}$$

Substitution of Eq. 58 into Eq. 65 then yields, after some manipulation

$$\frac{(\overline{\psi u})_m}{(\overline{\psi u})_o} = \left(\frac{2}{\sqrt{\pi}}\right)^{1-j} \left(\frac{D}{2C_\psi x}\right)^{j+1} G(\eta) \tag{59}$$

in which

$$G(\eta) = \frac{(1-\eta)^{\left(\frac{1-\eta}{4\eta}\right)^2}}{(1+\eta)^{\left(\frac{1+\eta}{4\eta}\right)^2}} \tag{60}$$

As η becomes very small (the maximum flux approaches the free surface) Eq. 58 may be simplified to

$$\frac{x_s}{z_o} = \frac{\sqrt{2}}{C_\psi + \sqrt{2}\,\theta} \tag{61}$$

in which x_s is the value of x for which $z_m = 0$. Note that for the usual range of values of C_ψ small values of θ have a large influence on x_s.

Letting

$$f(\eta) = \left(\frac{2}{\eta \text{ arc tanh } \eta}\right)^{1/2} \tag{62}$$

manipulation of Eq. 57 and Eq. 58 yields

$$\frac{z_m}{z_o} = \frac{\eta}{1 + \frac{\theta}{C_\psi} \eta \, f(\eta)} \tag{63}$$

and

$$\frac{x}{z_o} = \frac{1}{C_\psi} \frac{z_m}{z_o} f(\eta) \tag{64}$$

Since η lies between 0 and 1, selection of various values of η between these limits for specified values of C_ψ, x_o and θ will permit computation of the locus of the filament of maximum flux using Eq. 62, Eq. 63 and Eq. 64.

John, Mahajan and Kanbour (15) plot the decay of maximum velocity in the downstream direction for a submerged jet in a narrow channel in Fig. 9 of Ref. 15. Using this plot the spread coefficient for momentum flux is estimated to be $C \approx 0.101$. Moreover, from Fig. 8 for $x/D = 240$ C may be estimated to lie between 0.094 and 0.104. From Fig. 3 of Ref. 15 the initial behavior of the filament of maximum flux indicates that $\theta = 0$. For convenience, assuming a value of $C \approx 0.1$, Eq. 61 indicates that $x_s/z_o = 14.14$ for all submergences. This is in radical disagreement with the data in Fig. 3 of Ref. 15 from which $x_s/z_o = 2.50, 2.00, 2.00, 1.67$ and 1.50 for slot submergences $z_o/D = 16, 32, 48$ and 96 respectively. Such gross disagreement is surprising in view of the relatively good

agreement for the shallow submerged circular jet (2). The explanation, however, may be found in the text of Ref. 15, which states:

" .... . This means that some of the fluid is trapped in a region bounded by the wall containing the slot, the free surface and the upper periphery of the jet. This will set up vortices in the surrounding fluid. Owing to the back flow and the vortices set up in the region, the pressure will be considerably lower above the jet than below the jet, and hence, as a result there will be a net lift force which will cause the jet to deflect (as a whole) towards the free surface."

That the lift force described had considerable influence is substantiated by the fact that John, Mahajan and Kanbour found that the filament of maximum flux was the same, whether the effluent was at the same temperature as the receiving water or at a temperature 50^{o} higher for submergences less than $z_o/D = 120$. (Refer to Fig. 3 of Ref. 15.)

Although similar backflow behavior was observed for the shallow submerged circular jet (1), the reduction of pressure above the jet could be relieved by flow of water into the region from the sides. One might expect therefore, that the analysis given here might apply well to the central portion of a long slot outlet with no side boundaries to restrain lateral inflow into the region above the jet. Such a situation would more realistically represent the conditions near the outlet from a thermal power station. Some caution should be exercised in interpreting results collected in narrow laboratory channels for application to such prototype situations. It is very likely, that in the absence of lateral restraint on the flow the lift effect on the jet would be substantially reduced and the buoyancy effect for a heated effluent would be of much greater importance than the observations of Ref. 15 would indicate. On the other hand construction of

lateral wing walls to cut off lateral flows might be considered for prototypes.

If one is willing to modify the momentum spreading coefficient and the origin correction to account for the lift force present in the Ref. 15 results substantial agreement can be achieved between the data and Eq. 61, Eq. 62, Eq. 63 and Eq. 64. This in effect presumes that two different spreading coefficients will apply and is of questionable validity. The results of such a modification are summarized in Table 3 and Fig. 8. In view of the doubtful validity of this procedure no attempt was made to model the temperature data of Ref. 15 using the present analytic model. The data points shown in Fig. 8 are for both the heated and unheated jet at each submergence.

TABLE 3 — QUASI-MOMENTUM FLUX COEFFICIENTS AND ZERO CORRECTIONS FOR SHALLOW SLOT JET DATA

z_o/D	C	x_o/z_o
16	0.436	-1.33
32	0.518	-1.09
48	0.577	-0.84
72	0.643	-0.84
96	0.689	-0.80

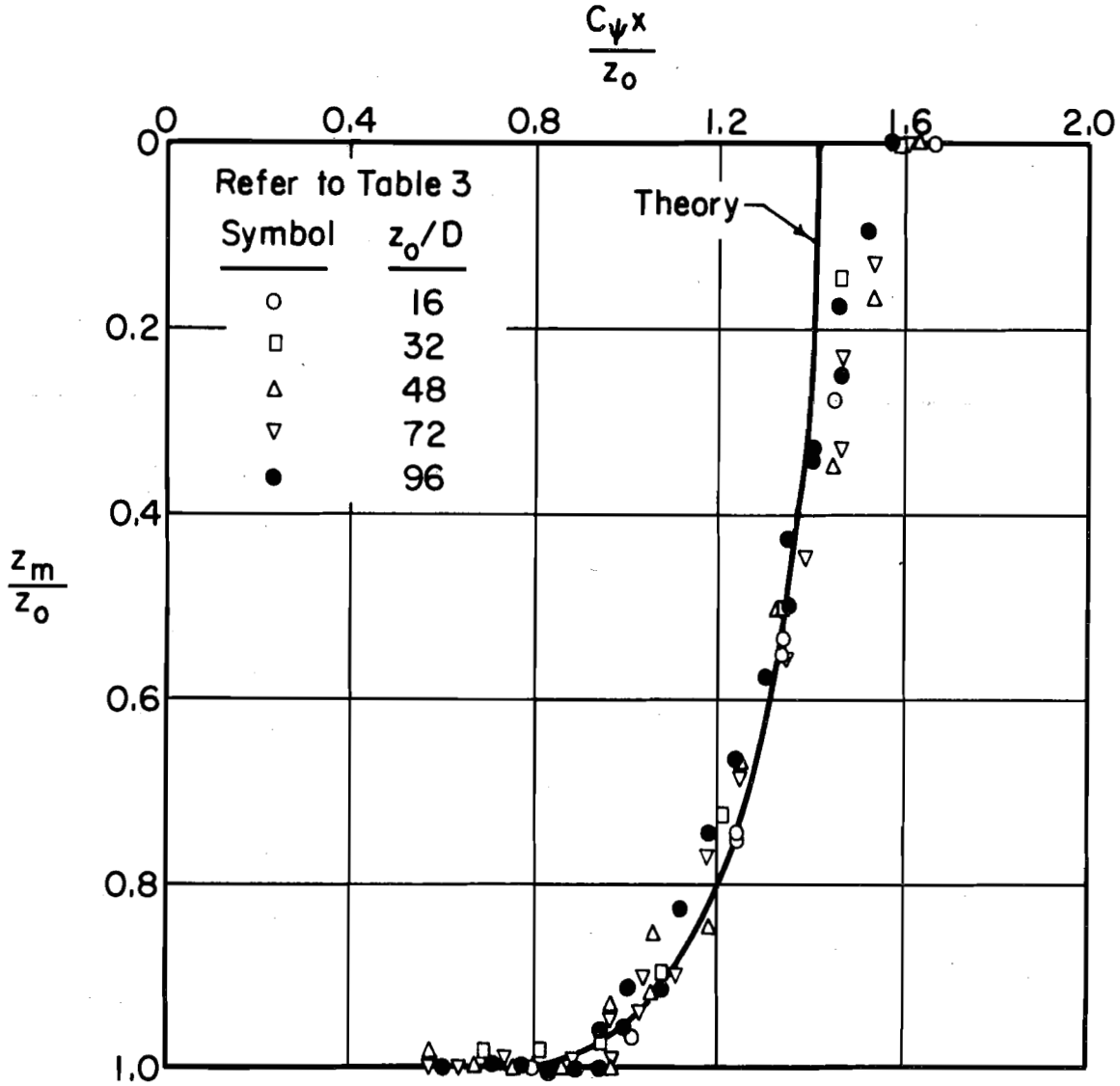

Fig. 8 - Filament of Maximum Flux for Heated and Unheated Laterally Confined Shallow Submerged Slot Jets

VII. THE P-FUNCTION APPLIED TO AXISYMMETRIC FLOWS

For a circular nozzle outlet of finite size, having a uniform distribution of initial flux, Eq. 37 gives the flux distribution (2, 3, 5)

$$\frac{\overline{\Psi u}}{(\overline{\Psi u})_o} = \int_o^{2\pi} \int_o^{\frac{D}{2}} \frac{\exp\left[-\frac{(y^2+s^2-2ys\cos\gamma)}{C_\Psi{}^2 x^2}\right]}{\pi C_\Psi{}^2 x^2} \, s\,ds\,d\gamma \qquad (65)$$

in which (s, γ) is a system of polar co-ordinates in the plane of the nozzle discharge and D = nozzle diameter.

As noted earlier this is the cumulative distribution function of the non-central chi-square distribution for which the chi-square, the first-normal and the second-normal approximations can be used (2,33).

H. H. Germond (16) used this same integral in military coverage problems to determine the probability that a missile will hit a circle of specified radius if it is aimed at a point a specified distance from the center of the circle and if it is subject to a Gaussian probability impact law of unit standard deviation; or to determine the probability that a missile aimed at a point a specified distance from a given point will hit within a specified distance of that point. He referred to the integral as the "circular coverage function" and presented a set of tables. It has also been called the "off-set circular probability function" (17).

Masters (17) called the same integral the "P-function", P(R, r), and discussed its mathematical properties and its application to problems of multiple scattering and classical diffusion theory. Hence, in Masters

notation

$$\frac{\overline{\psi u}}{(\overline{\psi u})_o} = P\left(\frac{D}{\sqrt{2}\, C_\psi x}, \frac{\sqrt{2}\, y}{C_\psi x}\right) \tag{66}$$

Masters (17) also defined the normalized P-function, $P^*(R, r)$ and tabulated it

$$P^*(R, r) = P(R, r)/P(R, o) \tag{67}$$

Hence

$$\frac{\overline{\psi u}}{(\overline{\psi u})_m} = P^*\left(\frac{D}{\sqrt{2}\, C_\psi x}, \frac{\sqrt{2}\, y}{C_\psi x}\right) \tag{68}$$

For values of $R > 3$, Masters (17) showed that

$$P^*(R, r) \approx \frac{1}{2}\left\{1 - \operatorname{erf}\left(\frac{r-R}{\sqrt{2}}\right)\right\} \tag{69}$$

Moreover since

$$P(R, o) = \int_o^R \exp\left(-\frac{t^2}{2}\right) \cdot t\, dt \tag{70}$$

for $R > 3$

$$P(R, o) \approx 1.0 \tag{71}$$

Thus, for $R > 3$

$$P^*(R, r) \approx P(R, r) \approx \frac{1}{2}\left\{1 - \operatorname{erf}\left(\frac{r-R}{\sqrt{2}}\right)\right\} \tag{72}$$

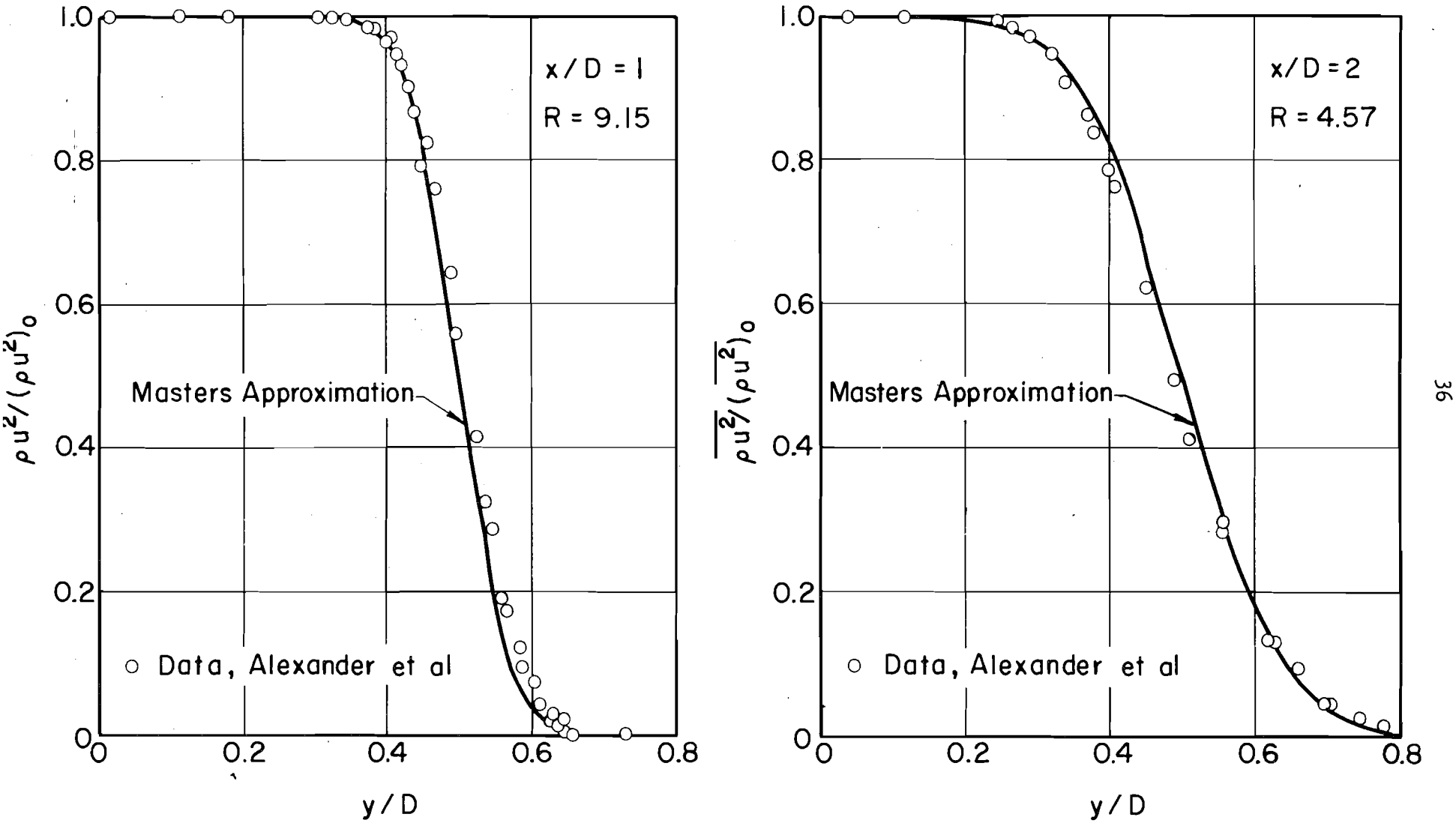

Fig. 9 - Master's Approximation of P-Function Compared with Radial Distribution of Momentum Flux Density Ratio for s/D = 1 and s/D = 2

For $R < 0.4$ the values of $P(R, r)$ are given by the Carlton approximation (16)

$$P(R, r) \approx \frac{R^2}{2+R^2/2} \exp[-r^2/(2+R^2/2)] \tag{73}$$

and

$$P^*(R, r) \approx \exp[-r^2/(2+R^2/2)] \tag{74}$$

Other available approximations are the chi-square, and the first and second normal approximations (18). These approximations were applied to jet momentum flux data in Ref. 2 and Ref. 3. The chi-square approximation was found to provide enough discrete points to adequately describe the flux distribution for values of $R > 3$. It is thus applicable in the same range as the Masters' approximation given by Eq. 72. The Masters' approximation is, however, much simpler to compute and gives a continuous representation of the distribution. Its application to axisymmetric jet momentum flux distributions is illustrated in Fig. 9 using the same data by Alexander et al (5) amployed with the chi-square approximation in Ref. 2 and Ref. 3. The first and second normal approximations which are tedious to compute could be applied over the range $0 < R < \infty$. Their application in the range $1.01 < R < 3$ was illustrated in Ref. 2 and Ref. 3 where it was found that the first normal approximation worked best for low values of r/R and the second normal for high values of r/R, the division between the two applications depending on R. The reader may refer to Fig. 5 of Ref. 2 or Fig. 4 of Ref. 3 for clarification of this point. Because of the tedious nature of the computations for the first and second normal approximations

use of tables (16, 17) for the P and P^* functions or of other approximations is preferable.

In Ref. 2 and Ref. 3 a much more useful approximation was obtained which was applicable at all points downstream from the potential core. Since Eq. 72 indicates that $P^*(R, r) \approx P(R, r)$ for $R > 3$ the limit $R = 3$ evidently represents the end of the potential core. Hence, in the range $0 < R < 3$ the following approximation is applicable

$$P^*(R, r) = \exp[-(\frac{r}{R})^2 \{1-\exp(-\frac{R^2}{2})\}] \tag{75}$$

and

$$P(R,r) = \exp[-(\frac{r}{R})^2 \{1-\exp(-\frac{R^2}{2})\}][1-\exp(-\frac{R^2}{2})] \tag{76}$$

Noting that, for $R < 0.4$

$$1 - \exp(-R^2/2) \approx R^2/(2+R^2/2) \approx \frac{R^2}{2}(1-R^2/4) \tag{77}$$

Eq. 75 and Eq. 76 are readily shown to reduce to the Carlton approximation for $R < 0.4$. Moreover, as R approaches zero (x becomes very large) the Carlton approximation approaches the solution for the point source jet

$$P(R, r) = \frac{R^2}{2} \exp(-r^2/2) \tag{78}$$

and

$$P^*(R, r) = \exp(-r^2/2) \tag{79}$$

The approximation given by Eq. 75 and Eq. 76 has been illustrated in Ref. 2 and Ref. 3 for the range $1 < R < 3$.

The available approximations to the P and P^* functions are summarized in Table 4. The approximations recommended for ease of computation in the various ranges are summarized in Table 5. Of course, as an alternative to any of these approximations the tables (16, 17) for the P and P^* functions may be used.

TABLE 4 — RANGE OF APPLICATION OF APPROXIMATIONS TO P-FUNCTION

Range of application		Approximation
R	$C_\psi x/D$	
$3 < R < \infty$	$0 < C_\psi x/D < 0.236$	Masters approximation $P(R,r) = P^*(R,r) = \frac{1}{2}[1-\text{erf}(\frac{r-R}{\sqrt{2}})]$
$3 < R < \infty$	$0 < C_\psi x/D < 0.236$	Chi-square approximation $P(R,r) = [2^{\frac{\nu}{2}} \Gamma(\frac{\nu}{2})]^{-1} \int_0^{R^2} t^{\frac{\nu}{2}-1} \exp(-\frac{t}{2}) dt$ with $\nu = \frac{(2+r^2)^2}{2(1+r^2)}$
$0 < R < \infty$	$0 < C_\psi x/D < \infty$	First normal approximation (small r/R) $\zeta = [\{\frac{R^2}{2+r^2}\}^{1/3} - 1 + \frac{2}{9\nu}]/\sqrt{\frac{2}{9\nu}}$ Second normal approximation (large r/R) $\zeta = [\frac{2\nu R^2}{2+r^2}]^{1/2} - [2\nu-1]^{1/2}$ with ν defined above $P(R,r) = \frac{1}{\sqrt{2\pi}} \int_{-\infty}^{\zeta} \exp(-t^2/2) dt$
$0 < R < 3$	$0.236 < C_\psi x/D < \infty$	Maxwell approximation $P^*(R,r) = \exp[-(\frac{r}{R})^2 \{1-\exp(-R^2/2)\}]$ $P(R,r) = [1-\exp(-R^2/2)] P^*(R,r)$
$0 < R < 0.4$	$1.768 < C_\psi x/D < \infty$	Carlton approximation $P^*(R,r) = \exp[-r^2/(2+R^2/2)]$ $P(R,r) = \frac{R^2}{2+R^2/2} P^*(R,r)$
$R \to 0$	$C_\psi x/D \to \infty$	Point source approximation $P^*(R,r) = \exp(-r^2/2)$ $P(R,r) = \frac{R^2}{2} P^*(R,r)$

TABEL 5 — RECOMMENDED APPROXIMATIONS AND RANGES OF APPLICATION TO P-FUNCTION

Approximation	Recommended range of application	
	R	$C_\Psi x/D$
Masters approximation	$3 < R < \infty$	$0 < C_\Psi x/D < 0.236$
Maxwell approximation	$0.4 < R < 3$	$0.236 < C_\Psi x/D < 1.768$
Carlton approximation	$0 < R < 0.4$	$1.768 < C_\Psi x/D < \infty$
Point Source approximation	$R \rightarrow 0$	$C_\Psi x/D \rightarrow \infty$

VIII. SUMMARY, CONCLUSIONS AND APPLICATIONS

Attempts to adapt the method of synthesis based on a generalization of Reichardt's hypothesis to describe flux profiles near fixed boundaries were unsuccessful. They are described in Section II of the report. Consequently, emphasis was placed on synthesizing diffusion patterns away from fixed boundaries. These included co-axial and co-planar flows, diffusion patterns downstream from outlets of different shapes, the effect of the initial distribution of flux at an outlet on the downstream flux patterns, shallow submergence effects on flows from two-dimensional slots and use of the P-function to model axisymmetric flux patterns.

The method of synthesis could be successfully applied in modelling co-axial and co-planar flows. It is, therefore, a promising tool for predicting the diffusion of tracers in penstocks, for example.

The effect of initial non-uniform distributions of flux were found to be damped out downstream from circular and slot outlets for $C_\psi x/D > 1.5$. For example, for momentum flux and circular outlets, $C_\psi \approx 0.08$. Thus the effects are indistinguishable beyond about 19 diameters downstream from the point of efflux. The effect of outlet shape was found to be much more persistent, extending to about 63 equivalent diameters for the shapes considered. This would indicate, that in modifying outlets to achieve desired diffusion patterns greater emphasis should be placed in exploring variations in outlet cross-sectional shape rather than in modifying the conduit geometry upstream from the outlet to achieve any particular flux distribution at the point of discharge.

Although the method of synthesis had been found to provide good predictions for momentum flux distributions downstream from a shallow submerged circular outlet it was found to be in substantial disagreement with recently published laboratory data for a shallow submerged slot placed across the end of a narrow channel. A vortex was trapped in the region above the effluent periphery, creating negative pressures which drew the jet up to the free surface much more rapidly than was predicted by the theory. The effect was sufficiently great to override any effects due to density difference between the effluent and the ambient fluid. For submergences up to 96 times the height of the slot there was no substantial difference in the behavior of an effluent 50 F° above ambient, and one at ambient temperature. The theory could be expected to provide agreement with data for a situation in which fluid could center the region above the jet from the sides to relieve the lowered pressures created by the trapped vortex. The comparison indicates, however, that effluents from thermal power plants could be made to rise to the surface much more rapidly by using wing-walls extending into the lake or reservoir in combination wtih slot outlets to insure that a vortex would be trapped above the emerging effleunt.

This same principle could be applied in the design of ocean outfalls to inhibit the effluent from rising to the surface. By using a long narrow slot outlet with wing walls a vortex could be trapped between the lower periphery of the effluent and the bed causing the effluent to adhere to the bed for some distance before rising to the surface.

It should be noted also that the analytic model based on the method of synthesis indicates that very small initial angles of inclination of the outlet have large effects on flux patterns for shallow submerged outlets.

Finally, four simple approximations to the P-function, involving only exponential and error functions, were found. Using these the mass, heat or momentum flux distribution downstream from a circular outlet of finite size with an initially uniform flux distribution can be rapdily computed at all points between the nozzle and infinity.

LIST OF REFERENCES

1. Maxwell, W.H.C., and Pazwash, H., "Basic Study of Jet Flow Patterns Related to Stream and Reservoir Behavior," Univ. of Illinois Water Res. Center Research Rpts., No. 10, July 1967, 63 pp.

2. Maxwell, W.H.C., and Pazwash, H., "Boundary Effects on Jet Flow Patterns Related to Water Quality and Pollution Problems," Univ. of Illinois Water Res. Center Research Rpts., No. 28, Jan. 1970, 84 pp.

3. Maxwell, W.H.C., "Flux Development Region in Submerged Jets," Proc. ASCE, Jl. of Eng. Mech. Div., Vol.96, No. EM6, Dec. 1970, pp. 1061-1079.

4. Reichardt, H., "On a New Theory of Free Turbulence," ZAMM, Vol. 21, No. 5, Oct. 1941 and translation by Flint, M., Jl. Roy. Aero. Soc., Vol. 47, 1943, pp. 167-176.

5. Alexander, L. G., Baron, T., and Comings, E. W., "Transportation of Momentum, Mass and Heat in Turbulent Jets," Univ. of Illinois Bulletins, No. 413, May 1953, 88 pp.

6. Tables of Integral Transforms, Erdelyi, A., ed., Vol. 1, McGraw-Hill Book Co. Inc., New York, 1954.

7. Papoulis, A., The Fourier Integral and its Applications, McGraw-Hill Book Co. Inc., New York, 1962.

8. Schlichting, H., "Turbulent Flow Through Pipes," Boundary Layer Theory, Chap. XX, Pergamon Press, New York, 1955, pp. 400-429.

9. Maczynski, J.F.J., "A Round Jet in an Ambient Co-axial Stream," Jl. of Fl. Mechs., Vol. 13, May-Aug. 1962, pp. 597-608.

10. Curtet, R. and Ricou, F. P., "On the Tendency to Self-Preservation in Axisymmetric Ducted Jets," Trans. ASME, Jl. of Basic Eng., Dec. 1964, pp. 765-776.

11. Ortega, J. J., "Characteristics of a Turbulent Round Jet in a Co-axial Stream," M.S. Thesis, Univ. of Iowa, 1968.

12. Bradbury, L.J.S., "The Structure of a Self-Preserving Turbulent Plane Jet," Jl. of Fl. Mechs., Vol. 23, Pt. 1, Sept. 1965, pp. 31-64.

13. Naudascher, E., "On the Distribution and Development of Mean Flow and Turbulence Characteristics in Jet and Wake Flows," Iowa Inst. for Hyd. Res. Rpts., No. 110, Aug. 1968.

14. Naudascher, E., "On a General Similarity Analysis for Turbulent Jet and Wake Flows," Iowa Inst. for Hyd. Res. Rpts., No. 106, Dec. 1967.

(List of References — cont'd)

15. John, J. E. A., Mahajan, B., and Kanbour, S., "Mixing Studies Associated with Thermal Pollution," Univ. of Maryland, Water Resources R s. Center Completion Report, Dec. 1970, 77 pp.

16. Germond, H. H., "The Circular Coverage Function," Rand Corp. Res. Mem., RM-330, Santa Monica, Cal., Jan. 1950, 16 pp.

17. Masters, J. I., "Some Applications in Physics of the P Function," Jl. of Chem. Physics, Vol. 23, No. 10, Oct. 1955, pp. 1865-1874.